J. Eng. Technol. Sci., Vol. 54, No. 5, 2022, 220503

Markerless Optical Motion Capture System for Asymmetrical Swimming Stroke

F. Ferryanto[1*], Andi Isra Mahyuddin[1] & Motomu Nakashima[2]

[1]Mechanical Design Research Group, Faculty of Mechanical and Aerospace Engineering, Institut Teknologi Bandung, Jalan Ganesa No. 10 Bandung 40132, Indonesia
[2]Department of Systems and Control Engineering, Tokyo Institute of Technology, Tokyo, Japan
*E-mail: ferryanto@ftmd.itb.ac.id

Highlights:

- The developed system does not require any particular configuration of camera and marker in recording the swimming motion.
- The developed system could capture the joint motion of an asymmetrical swimming stroke with insignificant error.
- The human body was modeled as a 15-segment model.
- An adaptive Gaussian Mixture Model was employed in the image segmentation step.
- The obtained joint motion was further analyzed by Swimming Human Simulation Model (SWUM) software to obtain the fluid forces.

Abstract. This work presents the development of a markerless optical motion capture system of the front-crawl swimming stroke. The system only uses one underwater camera to record swimming motion in the sagittal plane. The participant in this experiment was a swimmer who is active in the university's swimming club. The recorded images were then segmented to obtain silhouettes of the participant by a Gaussian Mixture Model. One of the swimming images was employed to generate a human body model that consists of 15 segments. The silhouette and model of the participant were subjected to an image matching process. The shape of the body segment was used as the feature in the image matching. The model was transformed to estimate the pose of the participant. The intraclass correlation coefficient between the results of the developed system and references were evaluated. In general, all body segments, except head and trunk, had a correlation coefficient higher than 0.95. Then, dynamics analysis by SWUM was conducted based on the joint angle acquired by the present work. The simulation implied that the developed system was suitable for daily training of athletes and coaches due to its simplicity and accuracy.

Keywords: *asymmetrical swimming stroke; front crawl; image matching; image processing; markerless optical motion capture.*

Received December 9th, 2021, Revised March 29th, 2022, Accepted for publication April 28th, 2022.
 ISSN: 2337-5779,
DOI: 10.5614/j.eng.technol.sci.2022.54.5.3

.

1 Introduction

Human swimming is a motion in water that generates propulsive force. Since humans are not born with the ability to swim naturally, this kind of motion is utterly complex. In sport, swimming competitions have been organized since the 19th century and possibly for many centuries before that. Swimmers in competition should obtain maximum speed and reduce drag force from the water as much as possible. Hence, swimming athletes require years of training, especially in movement coordination, to minimize energy use.

In swimming training for competition preparation, swimming motion has to be measured and analyzed. Measurement of swimming motion can be conducted by using an optical motion capture system. In an optical motion capture system, the swimming motion performed by the subject is recorded using a camera to obtain the joint trajectories. The joint trajectories are analyzed further to obtain kinematic and kinetic parameters of swimming motion, which are very useful in athletes' daily training.

Currently, a marker-based technique of optical motion capture is the most common technique used in motion analysis because of its relatively high accuracy [1-2]. The marker-based optical motion capture system is widely used in human movement analysis, mainly in gait analysis [3-4]. Moreover, the marker-based optical motion capture system is also used in swimming movement analysis. Monnet, *et al.* analyzed the feasibility of this system in measuring three-dimensional hand kinematics during swimming [5]. However, the marker-based technique has some limitations despite its accuracy; for example, the markers attached to the subject could affect the subject's movements. In addition, the experimental environment has to be controlled so that the time required for marker placement could be excessive [6]. Another limitation of the marker-based technique is the difficulty of discriminating the markers and mislabeling of the markers in automatic tracking. These problems could be solved by utilizing different colored LED markers. However, the color of LED cannot be distinguished underwater [7].

To overcome the limitation of the marker-based technique, markerless optical motion capture systems have been developed. In a markerless optical motion capture system, subjects do not have to use markers so that the process of the experiment can be more straightforward and manageable. Therefore, in the last decade, the development of markerless motion capture systems has been a highly active research area. This motion analysis method has been applied broadly in gait analysis [8-9]. Recently, a system has been introduced that can detect human joint motion without any markers required, using a neural network approach called OpenPose [10].

Although markerless gait analysis has been studied extensively, markerless optical motion capture systems for underwater application have not been investigated widely. While OpenPose is robust in detecting joint motion, there is no evidence that it can be used for underwater application. In 2011, Ceseracciu, *et al.* developed a markerless optical motion capture system to analyze the front-crawl stroke utilizing six cameras [11]. However, the complexity of the six camera locations was a main drawback of the research. Then, Ferryanto & Nakashima developed a markerless system to investigate the dynamics of the butterfly stroke for daily training use in 2017 [12]. The developed method could be used to study any bilaterally symmetric motion. However, the application of the developed system for asymmetrical swimming strokes was still in question. The main reason for this limitation is the number of links in the human body model, and it cannot distinguish the right and left sides of the body segment. Hence, the main objective of the present work was to improve the developed system so it can be used to obtain joint angle and dynamics parameters for asymmetrical swimming strokes. The improvement of the present study was the adjustment of the human body model and the inclusion of an algorithm to identify the right and left body segments. As a case study, the front-crawl stroke motion was investigated in the experiment for markerless analysis. The main contribution of the developed system is to decrease the required time to analyze the swimming movement, especially asymmetrical strokes. Compared to manual digitizing, which can take several days, the system could obtain the front-crawl kinematics data in just one hour.

2 Methodology

In the present work, an experiment to obtain the motion of front-crawl swimming was conducted. The participant in this experiment was a 23-year-old male swimmer who was active in the university's swimming club, with a height of 170.5 cm and a weight of 56.5 kg. The swimming speed in this experiment was 1.13 m/s. An underwater camera Nikon Coolpix AW110 with a resolution of 1280 x 760 pixels and a rate of 60 frames per second was located 4.5 m from the right side of the participant and 0.75 m below the water surface. No special lighting equipment is required in the image acquisition. The camera should be able to capture a minimum of two strokes of swimming in the sagittal plane. Figure 1 shows the swimming images recorded by the camera. Since the front-crawl stroke is defined by the arm movement, one swimming stroke cycle was defined by observing the swimming images. The pose of the participant silhouette at $t = 0.00$ and $t = 1.00$ should be identical to the indicator of one swimming cycle.

After recording the swimming motion, the next procedure was image segmentation, human body model generation, image matching, and identification

.

of right and left limb. A detailed description of each step will be presented in the following section.

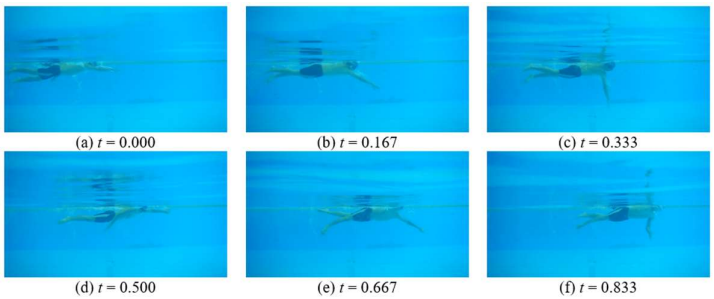

Figure 1 RGB swimming images. Each frame was described in non-dimensional time normalized by the cycle time.

2.1 Human Body Model Generation

Since human movement has many degrees of freedom, a human body model is required. The model contains a priori information about the participant's body shape to be matched with real images of the participant [13-14]. As a result, the movement of the participant's body segments could be obtained.

Human body models can be generated from a morphological description of the human body's anatomy [15]. The best way to generate a model is from direct measurement of the participant's outer body surface. Therefore, the model in this research was extracted from a swimming frame that included all body segments. Manual image segmentation was conducted to exclude the participant's body segments from the environment. There were 15 body segments, which were numbered i = 1 to 15 in the present model, i.e., head, trunk, hip, right and left thigh, right and left shank, right and left foot, right and left upper arm, right and left forearm, and right and left hand, as presented in Figure 2.

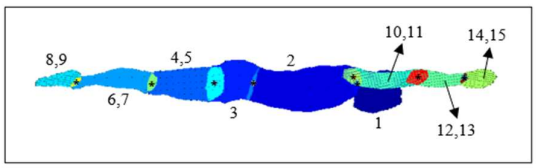

Figure 1 The generated model to assist the image matching process. The * marks indicate joints between two segments.

Joint positions should also be defined in the model as the center of rotation of each body segment. The joint positions can be obtained from the centroid of the

intersection of two segments. The * mark indicates the positions of all joints in the present model in Figure 2.

2.2 Image Segmentation

In this procedure, the silhouette of the participant was obtained to be used for the image matching step. The input for the image segmentation procedure were RGB images that were extracted from the recorded video of the participant swimming. The image segmentation process for swimming application is made more challenging due to bubbles resulted from the flutter kick. Therefore, in the present work, the image segmentation was conducted using an adaptive background Gaussian Mixture Model (GMM) [16].

In the application, the blue channel of RGB was used in the image segmentation procedure since the participant's silhouette has the most contrast against the background in the blue channel. Then, the intensity value of the bubbles was modeled as a GMM component, so that the bubbles could be interpreted as background. To enhance the image quality, a morphological operation was applied. The results of image segmentation are presented in Figure 3. The higher accuracy of the image segmentation increases the accuracy of the developed system. One of the methods to enhance the system's accuracy is to increase the participant's contrast with the environment. Hence, the accuracy of the image segmentation could be improved.

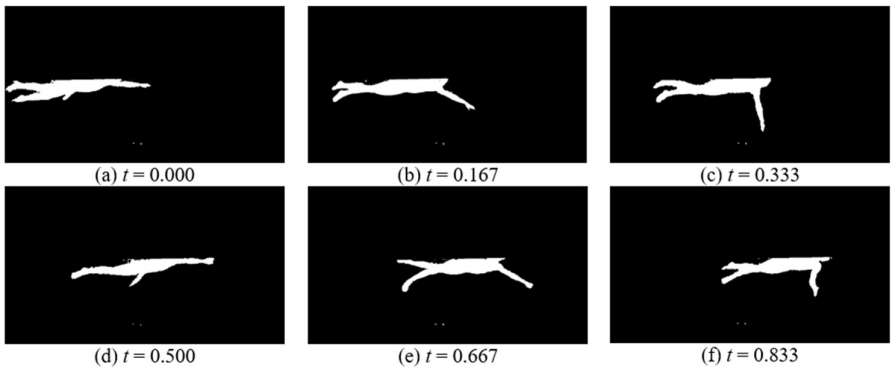

Figure 2 Silhouettes of the participant resulted from the image segmentation process. Each frame is in non-dimensional time.

2.3 Image Matching

The following procedure after generating the human body model and reconstructing the swimming image was to match the model to the swimming images to track the participant's movement. All body segments in the model are

.

transformed to align with the human body in the swimming images. The outcome of the image matching procedure is the participant's pose estimation, i.e., the rotation angle of each body segment.

In developing the image matching algorithm, proper features must be selected. The features in the image matching are objects that can be used to establish correspondence between two images [17], i.e., the human body model and the swimming images. The features must be easily detectable in both the model and the swimming images [18]. In general, the feature applied in the present matching algorithm is the shape of the human body in the model and swimming images. The shape of the human body was selected as the feature in this study because it is independent of changes in illumination [19].

The features detected in the model were then mapped to the swimming images by maximizing the similarity measure. The similarity measure used in this study was the intensity value between the mapped model and the swimming images. Thus, the intensity value of each pixel of the swimming images and the transformed model was investigated. If they had the same intensity value, then the similarity increased. This similarity measure was assessed only for the area below the water surface because the silhouette was only in this area.

The body segments were assumed to be rigid, with no change in shape occurring. Then all the body segments of the model were transformed using both translational and rotational parameters. The algorithm of image matching here was adapted from the algorithm in Ferryanto & Nakashima's work [12]. Initially, the trunk of the model ($i = 2$) was translated and rotated by parameters $\mathrm{t} = [t_x\ t_y]^{\mathrm{T}}$ and θ_2. Then, the other segment bodies were translated according to the location of the trunk to preserve the kinematic links. After the joints were connected, the other body segments were rotated by angle θ_i about each proximal joint.

Mathematically, the model could be expressed as $\mathrm{m} = \{\mathrm{x}_i\}_{i=1}^{15}$, where x_i denotes the pixel coordinate belonging to i-th body segment. The transformation of the model was written as

$$\bar{\mathrm{x}}_2 = \mathrm{R}(\theta_2)\mathrm{x}_2 + t \text{ for } i = 2 \quad (1)$$

$$\bar{\mathrm{x}}_i = \mathrm{R}(\theta_i)\mathrm{x}_i \text{ for } i = 1, \ldots, 15 \neq 2 \quad (2)$$

where $\bar{\mathrm{x}}_i$ denotes the pixel coordinate of the transformed i-th segment and $\mathrm{R}(\theta_i)$ is the rotation matrix with angle θ_i. Hence, the transformed model could be written as $\bar{\mathrm{m}} = \{\bar{\mathrm{x}}_i\}_{i=1}^{15}$. To obtain maximum pixel similarity between the transformed model and the swimming data, all transformation parameters $\mathrm{T} = [t_x\ t_y\ \theta_i]^{\mathrm{T}}$ were optimized by Eq. (3).

$$T = \underset{T}{\operatorname{argmin}} |\bar{m} - d| \quad (3)$$

where d denotes the silhouettes in the swimming images. The term $\underset{T}{\operatorname{argmin}} |\bar{m} - d|$ is the value of T that minimizes $|\bar{m} - d|$ [19].

The transformation parameters T in Eq. (3) were evaluated by an optimization procedure. Particle swarm optimization [20] was conducted to obtain the transformation parameter for segment *i* = 1 to 9 with the bound from -30 degrees to 30 degrees, excluding trunk and hip. Since the trunk and hip motion in the front-crawl stroke are limited, the lower and upper bound for both segments were taken as -15 degrees and 15 degrees, respectively.

Genetic algorithm optimization [21] was used to obtain the upper limb's rotation angle, i.e., segments *i* = 10 to 15, by solving Eq. (3). To decrease the degree of freedom in searching the optimum rotation angle of the upper limbs, the optimization by the genetic algorithm was bounded and constrained. The upper limb's motion was constrained by the speed of each upper limb and the rotation angle of the upper limb relative to their proximal limb.

2.4 Identification of Right and Left Limb

The result of the image matching algorithm was the rotation angle of all segments with right or left side unknown. Therefore, an additional algorithm to identify the right and left parts of the body was required. In identifying right and left limbs, the least distance approach was attempted. The least distance approach determined the right of the left limb based on the angle and angular velocity difference between two consecutive frames. The reason for this approach is that the body segments should move continuously in the front-crawl stroke. Hence, it is unlikely that the upper limbs rotate too fast or change direction suddenly.

3 Result and Discussion

In this section, the result of the developed markerless optical motion capture was validated. The validated rotation angles of the body segments and the body geometry were then used for dynamics analysis by Swimming Human Simulation Model (SWUM) to obtain the kinetic parameters of swimming. SWUM is software for dynamic analysis of swimming movements developed by Nakashima, *et al.* [22].

3.1 Image Matching

The accuracy of the image matching was measured by comparing the rotation angle obtained from the developed algorithm to the reference of the rotation

.

angle. As the reference for evaluating the image matching algorithm, the predefined human body model was manually aligned to the swimming images' silhouettes. In this procedure, alignment was conducted manually with the help of an especially developed graphical user interface (GUI). For reproducibility, another operator tested the developed GUI. Firstly, all segments were translated and rotated so that the trunk in the model was aligned perfectly with the silhouettes. Then, the transformation was continued to the other segments so that all segments were matched perfectly with the silhouettes of the participant in the swimming images. An example of the rotation angle obtained from manual matching and Eq. (3) is presented in Figure 4. As can be seen in Figure 4, the waveform of the rotation angle looks jagged, although a camera with 60 frames per second was used in the experiment. This jagged waveform means that not all the images were analyzed in the present study. Furthermore, the analyzed images were one-third of all images taken alternately to reduce the computational time.

Several body segments are above the water surface in the manual matching process, especially the head, feet, upper arms, forearms, and hands. The rotation angle of these segments was predicted by smoothing spline curve fitting [23]. The accuracy of the predicted rotation angle of segments above the water surface is not important because there is no interaction force between the body and the water. Therefore, it has no effect on the kinematic and kinetic parameters of front-crawl swimming.

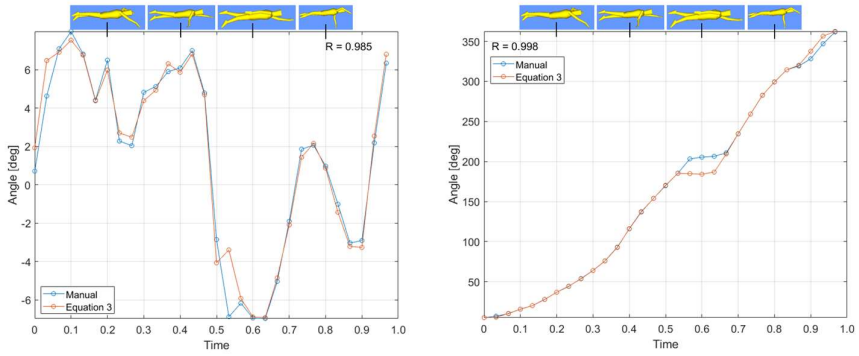

(a) (b)

Figure 3 Rotation angle obtained from the developed system for body segments: (a) right thigh, and (b) right upper arm.

In comparing the rotation angle obtained from the developed algorithm to the reference of the rotation angle, an intraclass correlation coefficient, *ICC*, and root mean squared error, *RMSE*, were calculated. The intraclass correlation coefficient measures the reliability of the developed system based on the analysis variance

and the estimation of variance between the rotation angle obtained from the image matching algorithm and the references [24]. The calculated *ICC* and *RMSE* are summarized in Table 1 for all body segments.

Table 1 The value of ICC and RMSE for all body segments. The RMSE in parentheses indicates an error of the body segment excluding the recovery phase.

i	Body Segment	Intraclass Correlation Coefficient, *ICC*	Root Mean Squared Error, *RMSE* (°)
1	Head	0.629	3.49
2	Trunk	0.812	0.46
3	Hip	0.941	0.26
4	Right thigh	0.984	0.83
5	Left thigh	0.994	1.06
6	Right shank	0.997	0.88
7	Left shank	0.991	1.33
8	Right foot	0.974	3.30
9	Left foot	0.978	4.55
10	Right upper arm	0.998	6.74
11	Left upper arm	0.999	1.70
12	Right forearm	0.969	28.30 (1.85)
13	Left forearm	0.914	48.17 (2.13)
14	Right hand	0.983	19.95 (14.21)
15	Left hand	0.966	29.65 (14.28)

The *ICC* values presented in Table 1 indicate that the developed algorithm in the present work produced acceptable results with the markerless optical motion capture system for daily training application. The developed system could also obtain the rotation angle of left body segments with a high correlation coefficient, even though the camera was placed on the participant's right side. The rotation angles of the left body segments were obtained from the image matching between the transformed model and the participant's silhouette. Since the silhouette of the left segments is visible in the images, the image matching algorithm could still be evaluated. The *ICC* was mostly larger than 0.95, except for the head and trunk. The head segment had a lower correlation coefficient because this segment was mainly outside the water. Hence, the head segment was not captured by the underwater camera. In addition, the trunk also had a lower correlation coefficient due to its insignificant movement in swimming. This is because, when the motion of the segment was very small, the fluctuation of the angle did not become a meaningful one but merely a measurement error.

Based on the *RMSE* value presented in Table 1, the rotation angle error obtained from the present system compared to those from manual matching was relatively minor. Therefore, it could be seen that the image matching algorithm was executed with good performance. In addition, the *RMSE* value in parentheses indicates an error when the recovery phase was excluded in the calculation. The

.

forearm and hand are above the water surface in the recovery phase, so the camera cannot capture them. Hence, their rotation angles were predicted by a curve fitting algorithm that resulted in a relatively large *RMSE*. However, this error did not affect the dynamics analysis because no propulsive force is produced in the recovery phase. In addition, the *RMSE* of the hand was comparatively large, although the rotation angle obtained from the curve fitting algorithm was excluded. The errors were caused by the blurred image, especially in the hand area, so the silhouette of the participant's hand was not segmented perfectly.

3.2 Dynamics Analysis by SWUM

For dynamic analysis using SWUM, the linear velocity at the center of gravity (CoG) of the participant was required as input. The linear velocity at the CoG was obtained from the world coordinates of the CoG after camera calibration with the Direct Linear Transformation method [25]. Apart from these data, body geometry and joint motion for each segment of the subject's body were also needed. The participant's height and weight in this study were 170.5 cm and 56.5 kg.

The human body model in the SWUM software originally consisted of 21 segments. The rotation angle of each segment was inputted separately. In this study, the human body was modeled as 15 segments. Thus, several body segments were combined in SWUM into one body segment. Thus, the SWUM software's rotation angle of the combined body segments was the same. For example, there is an upper and lower hip in the SWUM software. In the present study, the upper and lower hip was modeled by only one segment, i.e., the hip. Therefore, the inputted rotation angles of the upper and lower hip were identical.

An adjustment for the joint motion of each segment of the body to be included in SWUM was required. The joint motion obtained in this research was only in the sagittal plane. However, the front-crawl swimming stroke is a three-dimensional movement, especially the movement of the hands. The participant's hand in the front-crawl stroke has in an out sweep cycle. Therefore, the upper arm, lower arm, and hand rotation angles for the frontal and transverse planes needed to be defined, which was done using the joint motion available on http://www.swum.org/swumsuit/index.html. The inclusion of movement in the frontal and transverse plane from the available joint motion was conducted to show the capability of the system. Although the joint motion in the frontal and transverse plane was obtained from different swimmers, the calculation result is still useful for feedback to athletes and coaches since the sagittal plane motions are considered the most important in swimming. However, the user of this system does not always have to combine the obtained motion with different swimmers' motions. For example, the user can film the swimmer's motion from the front to

obtain the frontal and transverse motions first. Then, for daily training, the user can save time by using the pre-acquired frontal and transverse motions and combine them with sagittal motion observed on the training day.

The results of the dynamics analysis by SWUM are presented in Figure 5, respectively. Figure 5 shows the simulation result of the front-crawl stroke. The red line represents the vector of fluid forces acting on that segment. The propulsive force of swimming in the present work was mostly contributed by the upper limbs. The right upper limbs contributed around t = 0.167 to 0.5 to the propulsive force and the left upper limbs produced the same propulsive force at another time.

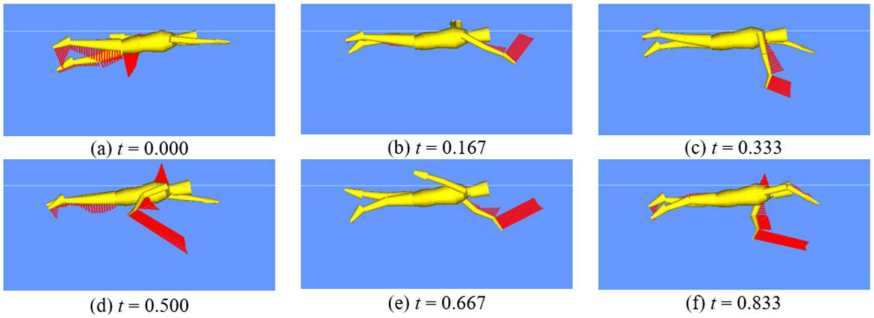

Figure 4 Result of the dynamics analysis by SWUM. The red line indicates the vector of fluid forces. Each frame is in non-dimensional time.

The interaction between the water and the participant's body segments resulted from the analysis of the dynamics by SWUM is important for the athlete and the coach. By investigating the propulsive forces, they can evaluate the athlete's movement and learn a strategy to increase the athlete's performance. Hence, the system developed in the present work is suitable for coaches and athletes for daily training use due to its simplicity in data acquisition of swimming movement. The present study's total computational time to analyze the front-crawl stroke was around one hour. The stroke investigated in the present study was the front-crawl stroke, but the current system can also be used to evaluate the other asymmetrical swimming strokes. In addition, the developed system is helpful in analyzing swimming motion of any level of swimmer, including top-level swimmers. One of the limitations of the present study is that the system could be improved to analyze in real-time, which could be the subject of future investigation. Moreover, the system should be validated for full-strength swimming, which may generate more bubbles.

.

4 Conclusion

The development of a markerless optical motion capture system for the front-crawl swimming stroke was presented. The system uses an underwater camera to acquire the motion of swimming. No configuration, such as lighting or marker attachment, is required. The system consists of image segmentation, model generation, image matching, and identification of right and left limb procedures. To validate the rotation angle of all body segments, the intraclass correlation coefficient (*ICC*) between the result and reference was investigated. It showed acceptable reliability of the system. The joint motion and body geometry of the participant was then used to obtain dynamics parameters of swimming using the SWUM software. From this result, coaches can evaluate the athlete's movement and learn a strategy to increase the athlete's performance. Hence, the developed system is suitable for coaches and athletes for daily training use due to its simplicity in data acquisition of swimming motion.

Acknowledgement

The authors gratefully acknowledge the support from the Japan International Cooperation Agency (JICA) and *Program Penelitian, Pengabdian kepada Masyarakat dan Inovasi* ITB (P3MI ITB) 2017.

References

[1] Windolf, M., Götzen, N. & Morlock, M., *Systematic Accuracy and Precision Analysis of Video Motion Capturing Systems - Exemplified on the Vicon-460 System*, Journal of Biomechanics, **41**(12), pp. 2776-2780, 2008.

[2] Maletsky, L.P., Sun, J. & Morton, N.A., *Accuracy of an Optical Active-Marker System to Track the Relative Motion of Rigid Bodies*, Journal of Biomechanics, **40**(3), pp. 682-685, 2007.

[3] Mihradi, S., Ferryanto, F., Dirgantara, T. & Mahyuddin, A.I., *Development of an Optical Motion-Capture System for 3D Gait Analysis*, 2nd International Conference on Instrumentation, Communications, Information Technology, and Biomedical Engineering (ICICI-BME), Bandung, 2011.

[4] Whittle, M.W., *Gait Analysis: An Introduction*, Butterworth-Heinemann, 2014.

[5] Monnet, T., Samson, M., Bernard, A., David, L. & Lacouture, P., *Measurement of Three-Dimensional Hand Kinematics During Swimming with a Motion Capture System: A Feasibility Study*, Sports Engineering, **17**, pp. 171-181, 2014.

[6] Corazza, S., Muendermann, L., Chaudhari, A.M., Demattio, T., Cobelli, C. & Andriacchi, T.P., *A Markerless Motion Capture System to Study Musculoskeletal Biomechanics: Visual Hull and Simulated Annealing Approach*, Annals of Biomedical Engineering, **34**, p. 1019-1029, 2006.

[7] Hernandez, Y., Kim, K.H., Benson, E., Jarvis, S., Meginnis, I. & Rajulu, S., *Underwater Space Suit Performance Assessments Part 1: Motion Capture System Development and Validation*, International Journal of Industrial Ergonomics, **72**, pp. 119-127, 2019.

[8] Goffredo, M., Carter, J.N. & Nixon, M.S., *2D Markerless Gait Analysis*, 4th European Conference of the International Federation for Medical and Biological Engineering, Berlin, Heidelberg, 2009.

[9] André, J., Lopes, J., Palermo, M., Gonçalves, D., Matias, A., Pereira, F., Afonso, J., Seabra, E., Cerqueira, J. & Santos, C., *Markerless Gait Analysis Vision System for Real-time Gait Monitoring*, 2020 IEEE International Conference on Autonomous Robot Systems and Competitions (ICARSC), 2020, Ponta Delgada, Portugal, 2020.

[10] Cao, Z., Simon, T., Wei, S.E. & Sheikh, Y., *OpenPose: Realtime Multi-Person 2D Pose Estimation using Part Affinity Fields*, IEEE Transactions on Pattern Analysis and Machine Intelligence, **43**(1), pp. 172-186, 2019.

[11] Ceseracciu, E., Sawacha, Z., Fantozzi, S., Cortesi, M., Gatta, G., Corazza, S. & Cobelli, C., *Markerless Analysis of Front Crawl Swimming*, Journal of Biomechanics, **44**(12), p. 2236-2242, 2011.

[12] Ferryanto, F., & Nakashima, M., *Development of A Markerless Optical Motion Capture System for Daily Use of Training in Swimming*, Sports Engineering, **20**, p. 63-72, 2017.

[13] Rosenhahn, B., Kersting, U.G., Smith, A.W., Gurney, J. K., Brox, T. & Klette, R., *A System for Marker-Less Human Motion Estimation*, Lecture Notes in Computer Science, Berlin, Heidelberg, Springer, 2005, pp. 230-237.

[14] Bouchrika, I. & Nixon, M.S., *Model-Based Feature Extraction for Gait Analysis and Recognition*, in Lecture Notes in Computer Science, Berlin, Heidelberg, Springer, pp. 150-160, 2007.

[15] Mündermann, L., Corazza, S. & Andriacchi, T.P., *The Evolution of Methods for the Capture of Human Movement Leading to Markerless Motion Capture for Biomechanical Applications*, Journal of NeuroEngineering and Rehabilitation, **3**(6), 2006. DOI: 10.1186/1743-0003-3-6.

[16] Zivkovic, Z., *Improved Adaptive Gaussian Mixture Model for Background Subtraction*, 17th International Conference on Pattern Recognition, 2004, Cambridge, UK, 2004.

[17] Goshtasby, A.A., *Image Registration: Principles, Tools and Methods*, Springer Science & Business Media, 2012.

.

[18] Zitova, B. & Flusser, J., *Image Registration Methods: A Survey*, Image and Vision Computing, **21**(11), pp. 977-1000, 2003.
[19] Schmidt, M, *Argmax and Max Calculus*, The University of British Columbia, https://www.cs.ubc.ca/~schmidtm/Documents/2016_540_Argmax.pdf, (6 January 2016).
[20] Wang, D., Tan, D. & Liu, L., *Particle Swarm Optimization Algorithm: An Overview*, Soft Computing, **22**, p. 387-408, 2018.
[21] Golberg, D. E., *Genetic Algorithms in Search, Optimization, and Machine Learning*, Addion Wesley, 1989.
[22] Nakashima, M., Satou, K., & Miura, Y., *Development of Swimming Human Simulation Model Considering Rigid Body Dynamics and Unsteady Fluid Force for Whole Body*, Journal of Fluid Science and Technology, **2**(1), pp. 56-67, 2007.
[23] Craven, P. & Wahba, G., *Smoothing Noisy Data with Spline Functions*, Numerische Mathematik, **24**, pp. 383-393, 1975.
[24] Bartko, J.J., *The Intraclass Correlation Coefficient as a Measure of Reliability*, Psychological Reports, **19**(1), pp. 3-11, 1966.
[25] Qingchao, W., GuoQing, Z., Qing, Z. & Qinghang, Z., *On DLT Method for CCD Camera Calibration,* Third International Conference on Signal Processing (ICSP'96), Beijing, China, 1996.